

Raman spectroscopic determination of the length, strength, compressibility, Debye temperature, elasticity, and force constant of the C-C bond in graphene

X. X. Yang,¹ J. W. Li,¹ Z. F. Zhou,¹ Y. Wang,² L. W. Yang,¹ W. T. Zheng,³ Chang Q. Sun^{1,4,*}

Abstract

From the perspective of bond relaxation and vibration, we have reconciled the Raman shifts of graphene under the stimuli of the number-of-layer, uni-axial-strain, pressure, and temperature in terms of the response of the length and strength of the representative bond of the entire specimen to the applied stimuli. Theoretical unification of the measurements clarifies that: (i) the opposite trends of Raman shifts due to number-of-layer reduction indicate that the G-peak shift is dominated by the vibration of a pair of atoms while the D- and the 2D-peak shifts involves z-neighbor of a specific atom; (ii) the tensile strain-induced phonon softening and phonon-band splitting arise from the asymmetric response of the C_{3v} bond geometry to the C_{2v} uni-axial bond elongation; (iii) the thermal-softening of the phonons originates from bond expansion and weakening; and (iv) the pressure- stiffening of the phonons results from bond compression and work hardening. Reproduction of the measurements has led to quantitative information about the referential frequencies from which the Raman frequencies shift, the length, energy, force constant, Debye temperature, compressibility, elastic modulus of the C-C bond in graphene, which is of instrumental importance to the understanding of the unusual behavior of graphene.

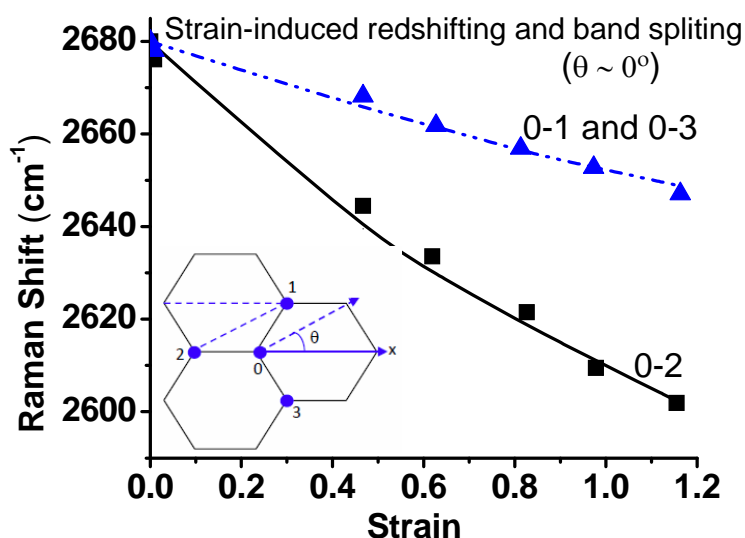
Keywords: graphene, Raman, bond, lattice dynamics

* Corresponding author. Tel: 65 6790 4517. Fax: +65 68733318. E-mail: ecqsun@ntu.edu.sg (Chang Q Sun)

Table of Contents

(For editor and referees' convenience only)

TOC art work



Raman spectroscopic determination of the length, strength, compressibility, Debye temperature, elasticity, and force constant of the C-C bond in graphene	1
Abstract	1
1. Introduction	6
2. Principles	9
2.1 BOLS correlation	9
2.2 The Raman shifts	11
2.3 Analytical solutions	11
2.4 Number-of-layer and strain dependence	14
2.5 Pressure and temperature dependence	16
3. Experimental and calculation procedures	17
4. Results and discussion	18
4.1 Number-of-layer dependence	18
4.2 Strain-induced red shifting and band splitting	20
4.3 Pressure and temperature dependence	22
4.4 Edge discriminative Raman reflectivity	23
5. Conclusion	24

¹Institute for Quantum Engineering and Micro-Nano Energy Technology, Key Laboratory of Low-Dimensional Materials and Application Technologies, and Faculty of Materials and Optoelectronic Physics, Xiangtan University, Hunan 411105, China

²School of Information and Electronic Engineering, Hunan University of Science and Technology, Xiangtan 411201, China;

³Department of materials Science, Jilin University, Changchun Changchun 130012, China

⁴School of Electrical and Electronic Engineering, Nanyang Technological University, Singapore 639798, Singapore

1. Introduction

Overwhelming contributions have been made in recent years with establishment of a huge database towards the lattice dynamics of the single- and the few-layer graphene and their nanoribbons (GNRs) under externally applied stimuli. The stimuli include the number-of-layer (n), [1, 2, 3, 4] uni-axial compressive and tensile strains (ϵ), [5, 6, 7] pressure (P), [8] temperature (T), [9, 10] defect density and location, [11] substrate interaction, [12, 13] hydrogenation, [14, 15] dopant, [16] incident photon polarization, [17] edge conditions, [18, 19] etc. A large graphene sheet manifests two Raman phonon modes: i) as the standard first-order approximation of Raman process, the G band ($\sim 1580 \text{ cm}^{-1}$) was suggested to arise from the in-plane vibration of the sp^2 carbon network; [20] ii) the 2D band (2680 cm^{-1}) was believed as a second-order process of double resonant Raman feature. [21] In the presence of undercoordinated defect or edge atoms, a defect-induced D band at frequencies around 1345 cm^{-1} can be resolved with intensity being varied with edge conditions. [18, 19]

The Raman shifts of graphene are very sensitive to the applied stimuli. The D and 2D bands undergo a redshift when the number-of-layer of the graphene is reduced and the Raman frequencies change with the energy of the incident radiation. [3, 22] Under 514.5 nm light radiation, the D mode shifts from 1367 to 1344 cm^{-1} and the 2D mode changes from 2720 to 2680 cm^{-1} when the bulk graphite evolves into the monolayer graphene. [4] In contrast, a blue shift happens to the G mode that shifts from 1582 to 1587 cm^{-1} when the n is reduced from 20 to one. [3, 4] When the n is increased from a few to multiple, the Raman peaks turn from the dominance of the monolayer component to the dominance of the bulk component. [3] The

opposite n-dependent trends indicate that the G mode and the D/2D modes are governed by different mechanisms though their origins remain to be clear.

When the graphene is under an uni-axial tensile strain[5] or heating,[23] the Raman peaks shift to lower frequencies. When pressure is increased, the Raman frequency shifts up sublinearly.[8] The uni-axial tensile strain can soften and split the G and 2D bands and the extent of the band splitting depends on the magnitude and the relative direction of the strain to the crystal orientation.[7, 24] Under the compressive strain, the Raman shift extrapolates the trend of the tensile strain.[25] It is even amazing that the spectral intensity of the D band is one order higher at the armchair edge than that at the zigzag edge of the GNR.[18, 19]

In order to describe the effect of P and T on the Raman shifts in general, the empirically quadratic functions are often used,[26, 27]

$$\begin{cases} \omega(T) = \omega(0) + \Delta\omega_e(T) + \Delta\omega_d(T) & (\text{Thermal softening}) \\ \omega(P) = \omega(0) + aP + bP^2 & (\text{pressure hardening}) \end{cases}$$

where $\omega(0)$ is the frequency measured at the ambient temperature and under the atmospheric pressure. The terms of $\Delta\omega_e(T)$ and $\Delta\omega_d(T)$ represent contributions from, respectively, the thermal expansion and the coupling of anharmonic phonons of multiple branches. In the P effect, the freely-adjustable parameters, a and b, are involved. A Grüneisen parameter, $\gamma = -\partial\omega/\partial\varepsilon$ or $\gamma_E = -\partial\ln\omega/\partial\ln\varepsilon$ has also been employed to describe the strain effect.[5] Recent density-functional theory calculations[24] suggested that the strain activates the processes of “two-phonon double-resonance scattering”, which are responsible for the strain-induced phonon band splitting and softening. Although the given empirical models could fit to the measurements independently, theoretically consistent formulation of the measurements remains challenging. In particular, the number-of-layer effect on the Raman shift remains theoretically unexplored.

Consistent insight into the mechanism behind the multiple-factor-stimulated Raman shift and, most strikingly, an extraction of quantitative information about the bonding identities from the sophisticated measurements are highly demanded and should be the provision of the sophisticated experiments.

A physical model should meet the following criteria and be able to:

- i) reproduce the measurements with meaningful parameters;
- ii) provide consistent insight into the physical mechanism behind observations;
- iii) extract quantitative information from the measurements; and,
- iv) establish the correlation between the measurements under various stimuli such as size, strain, pressure and temperature in the present course.

It is our thought that the external stimuli activate a certain set of intrinsic parameters that govern the Raman shift intrinsically. The vibration frequency should depend on the stimuli in a hidden form, instead. The relationship of the “vibration-intrinsic parameter-stimuli” is to be established. The objective of this contribution is to show that incorporating our original bond order-length-strength (BOLS) correlation theory[28, 29, 30, 31] to the Raman spectroscopy has enabled us to reconcile the effects of the number-of-layer, pressure, strain, and temperature on the Raman shifts of graphene. From the perspective of the local bond averaging (LBA) approach,[32] we focus on the formulation of the Raman shifts as a function of the order, length and strength of the representative bond of the entire specimen and their response to the applied stimuli. Agreement between the modeling predictions and the measurements has led to consistent insight into the mechanism behind the fascinations with revealing of quantitative information of the referential frequency $\omega(l)$ and its bulk shift, binding energy E_b , atomic cohesive energy E_{coh} , binding energy density E_{den} , Debye temperature θ_D , elastic modulus B , force constant k ,

compressibility β , and the effective coordination number (CN, or z) for the few-layer graphene and their bond lengths and energies, which is beyond the scope of available approaches.

2. Principles

2.1 BOLS correlation

Extended from the “atomic coordination–radius” correlation premise of Goldschmidt,[33] Pauling[34] and Feibelman[35] and experimental evidence [36, 37, 38, 39, 40] to include the bond energy response to the spontaneous contraction of the bonds between undercoordinated atoms, the BOLS correlation indicates that the shorter and stronger bonds between undercoordinated atoms cause local densification and quantum entrapment of bonding electrons and binding energy, which modulate the local atomic cohesive energy, the binding energy density, the Hamiltonian of the entire specimen and the relevant properties such as mechanical strength, thermal stability, lattice dynamics, photonic, magnetic and dielectric properties associated with atomic undercoordination.[28] Numerically, the BOLS correlation is expressed as

$$\begin{cases} d_z / d_b = C_z = 2 / \{1 + \exp[(12 - z)/8z]\} & (\text{bond contraction}) \\ E_z / E_b = C_z^{-m} & (\text{bond strengthening}) \end{cases} \quad (1)$$

The subscripts z and b denote an atom with z coordination neighbors and in the bulk as a standard, respectively. The bond contraction coefficient C_z varies only with the effective z of the atom of concern regardless of the nature of the bond or the solid dimension. The index $m = 2.56$ is the bond nature indicator of carbon.[30] Using the length of 0.154 nm for the C-C bond in diamond and 0.142 nm in graphite, one can readily derive the effective CN for the bulk graphite as $z_g = 5.335$, according to the bond contraction coefficient (eq 1). For the C atom in the bulk

diamond, the effective CN is 12 instead of 4 because the diamond structure is formed by an interlock of two fcc unit cells. By the relation of $E_z = C_z^{-m} E_b$, and the known atom cohesive energy of diamond, 7.37 eV,[41] the single C-C bond energy in the diamond is $E_b = 7.37/12 = 0.615$ eV and it is $E_3 = 1.039$ eV in the monolayer graphene of $z = 3$. The cohesive energy per atom in graphene is 3.11 eV/atom.

Theoretical reproduction of the elastic modulus enhancement,[30, 42, 43] melting point depression of the single-walled carbon nanotube (SWCNT),[30, 44] the C 1s binding energy shift of graphene edge, graphene, graphite, and diamond,[45, 46] the width dependence of the band gap expansion of GNR^[47] and the Dirac-Fermi polarons generation and hydrogenation[29] have confirmed consistently that the C-C bond at the graphene edge contracts by 30% from 0.154 to 0.107 nm with a 152% bond energy gain.[30, 42, 43] For the 3-coordinated GNR interior atoms, the C-C bond contracts by 18.5% to 0.125 nm with a 68% increase of bond energy.[42] The Young's modulus of the SWCNT was determined to be 2.595 TPa with respect to the bulk modulus of 865 GPa. The effective wall thickness of the SWCNT is determined to be 0.142 nm. The CN reduction-induced bond contraction is in good accordance with the supershort Cr-Cr dimer distance of 0.180 nm compared with that in the bulk of 0.254 ~ 0.270 nm.[48, 49] These findings agree well with what discovered by Girit et al[50] in their transmission electron microscopic study of the thermodynamic behavior of graphene. They found that breaking a C-C bond of the 2-coordinated carbon atom near the vacancy requires 7.50 eV per bond that is 32% higher than the energy (5.67 eV/bond) required for breaking one bond of a 3-coordinated carbon atom in a suspended graphene. These findings provide further evidence for the BOLS prediction of the shorter and stronger bonds between undercoordinated carbon atoms.

2.2 The Raman shifts

It is emphasized that the solution to the Hamiltonian of a vibration system is a Fourier series with multiple terms of frequencies being fold of that of the primary mode.[51] Therefore, the frequency of the secondary 2D mode should be twofold that of the primary D mode. This fact may clarify the origin of the 2D mode as commonly referred as the double resonant Raman process. Any perturbation to the Hamiltonian such as the interlayer Van der Waals force or the dipole-dipole interaction or the nonlinear effect may cause the folded frequencies to deviate from the ideal values. The fact that the number-of-layer reduction induced D peak shifting from 1367 to 1344 cm^{-1} and the 2D peak shifting from 2720 to 2680 cm^{-1} , is right within this expectation. The opposite trends of the Raman shifts due to the change of the number-of -layer indicate that the G mode is different from the D/2D mode in origin; therefore, one cannot expect to unify them simultaneously using an identical model. On the other hand, the applied strain, pressure, temperature or the atomic-CN variation can modulate the length and energy of the involved bonds, or their representative, and hence the phonon frequencies in terms of bond relaxation and vibration. Band splitting is expected to happen if the uni-axial strain is applied mismatching the graphene of C_{3v} group symmetry. The extent of band splitting under strain depends on the extent of the mismatch between crystal geometry and strain.

2.3 Analytical solutions

Generally, one can measure the Raman resonance frequency as $\omega_x = \omega_{x0} + \Delta\omega_x$ ($x = D, 2D, G$), where ω_{x0} is the reference point from which the Raman shift $\Delta\omega_x$ proceeds under the applied stimuli. The ω_{x0} may vary with the frequency of the incident radiation and substrate conditions but not the nature and the trends induced by the applied stimuli. By expanding the interatomic

potential in a Taylor series around its equilibrium and considering the effective atomic z , we can derive the vibration frequency shift of the harmonic system,

$$\begin{aligned}
u(r) &= \sum_{n=0} \left(\frac{d^n u(r)}{n! dr^n} \right)_{r=d_z} (r-d_z)^n \\
&\cong E_z + 0 + \frac{d^2 u(r)}{2! dr^2} \Big|_{r=d_z} (r-d_z)^2 + 0((r-d_z)^{n \geq 3}).. \\
&= E_z + \frac{\mu \omega^2 (r-d_z)^2}{2} + 0((r-d_z)^{n \geq 3}).....
\end{aligned}$$

From the dimensionality analysis, the term $\frac{\partial u(r)}{\partial r^2} \Big|_{r=d}$ is proportional to $\frac{E_z}{d^2}$. Equaling the vibration energy to the third term in the Taylor series and omitting the higher order terms, we have,

$$\frac{1}{2} \mu (\Delta \omega)^2 x^2 \cong \frac{1}{2} \frac{\partial u(r)}{\partial r^2} \Big|_{r=d} x^2 \propto \frac{1}{2} \frac{E_z}{d^2} x^2$$

As the first-order approximation, the lattice vibration frequency ω can be detected as Raman shift $\Delta \omega_x(z, d_z, E_z, \mu)$ from the reference point, $\omega_x(1, d_b, E_b, \mu)$, which depends functionally on the order z , length d_z , and energy E_z of the representative bond for the entire specimen and the reduced mass of the dimer atoms of the representative bond with $\mu = m_1 m_2 / (m_1 + m_2)$,

$$\begin{aligned}
\Delta \omega_x(z, d_z, E_z, \mu) &= \omega_x(z, d_z, E_z, \mu) - \omega_x(1, d_b, E_b, \mu) \\
&= \omega = \sqrt{\frac{d^2 u(r)}{\mu dr^2} \Big|_{r=d_z}} \propto \frac{1}{d_z} \left(\frac{E_z}{\mu} \right)^{1/2} \times \begin{cases} 1 & \text{(G mode)} \\ z & \text{(D/2D mode)} \end{cases}
\end{aligned} \tag{2}$$

The number-of-layer (coordination number) reduction induced D/2D mode redshift and the G mode blue shift suggest that the G mode be dominated by interaction between two

neighboring atoms while, as the double phonon resonance, the D/2D modes involve all the z neighbors of a specific atom. According to the BOLS, the E_z/d_z increases when the z is reduced, and hence blueshift happens, which is the case of the G mode; however, if the z is involved, the zE_z/d_z drops with z , which is right the case of the D and 2D mode under the reduction of the number-of-layer. This clarification may deepens our insight into the bond origin of the Raman active mode not only in graphene but also in TiO₂ [52] with the size induced abnormal blueshift of the 141 cm⁻¹ vibration.

The Raman shift $\Delta\omega_x(z, d_z, E_z, \mu)$ is a hidden function of the stimuli of T and P. For convenience, we may rename ω_{x0} as $\omega_x(1)$ that is to be obtained from matching theory to the measurements. The reduced mass of the dimer μ remains a constant unless chemical adsorption or isotope is being involved. Therefore, the Raman shift provides a powerful tool for detecting any change of the order, length, strength and the reduced mass of the representative bond for the specimen. Here we use the proportional relations based on the dimensionality analysis as we do not need the exact values of the hided constants in the numerical expressions in seeking for relative change of the concerned quantities. What we are concerned are the bonding origins of the Raman shifts and the quantitative information extracted from the sophisticated measurements.

Incorporating the variables of atomic coordination, strain, temperature, and pressure (z, ε, T, P) into the expressions (2), we have the general form of the relative Raman shift,

$$\frac{\omega(z, \varepsilon, P, T) - \omega(1, \varepsilon, P_0, T_0)}{\omega(z_b, 0, P_0, T_0) - \omega(1, 0, P_0, T_0)} = \frac{zd_b}{d(z, \varepsilon, P, T)} \left(\frac{E(z, \varepsilon, P, T)}{E_b} \right)^{1/2}$$

where

$$\begin{cases} d_b = d(z_b, 0, P_0, T_0) \\ E_b = E(z_b, 0, P_0, T_0) \end{cases}$$

$$\left\{ \begin{array}{l} d(z, \varepsilon, P, T) = d_0 \Pi_J (1 + \varepsilon_J) = d_b \left[(1 + (C_z - 1)) \left(1 + \int_0^\varepsilon d\varepsilon \right) \left(1 + \int_{T_0}^T \alpha(t) dt \right) \left(1 - \int_{P_0}^P \beta(p) dp \right) \right] \\ E(z, \varepsilon, P, T) = E_0 \left(1 + \sum_J \Delta_J \right) = E_b \left[1 + \frac{(C_z^{-m} - 1) - d_z^2 \int_0^\varepsilon \kappa(\varepsilon) \varepsilon d\varepsilon - \int_{T_0}^T \eta(t) dt - \int_{V_0}^V p(v) dv}{E_b} \right] \end{array} \right. \quad (3)$$

T_0 and P_0 are the references at the ambient conditions. Δ_J is the energy perturbation and ε_J the strain caused by the applied stimuli. The summation and the production are preceded over all the J stimuli of (z, ε, P, T) . The $\alpha(t)$ and $\beta(p)$ are, respectively, the thermal expansion coefficient and the compressibility. The $k(\varepsilon)$ is the effective force constant and $\eta(t)$ the specific heat of the representative bond. These expressions indicate that the mechanical work hardening by compression or by the compressive strain will shorten and strengthen but the thermal vibration or the tensile strain will elongate and weaken the C-C bond. Atomic CN reduction shortens and strengthens the C-C bond, according to the BOLS correlation. The generalized form indicates that we can consider all the stimuli either individually or collectively, depending on the experimental conditions.

2.4 Number-of-layer and strain dependence

Taking $z_g = 5.335$ for the bulk graphite as a reference, we can derive from eqs (2) and (3) the reference of $\omega_x(1)$ and the z -dependent frequency $\omega_x(z)$ for the possible Raman modes.

Letting

$$C_x(z, z_g) = \frac{\omega_x(z) - \omega_x(1)}{\omega_x(z_g) - \omega_x(1)} = \left(\frac{C_z}{C_{zg}} \right)^{-(m/2+1)} \times \begin{cases} \frac{z}{z_g} & \text{(D and 2D)} \\ 1 & \text{(G mode)} \end{cases},$$

We have,

$$\begin{cases} \omega_x(1) = \frac{\omega_x(z) - \omega_x(z_g)C_x(z, z_g)}{1 - C_x(z, z_g)} \\ \omega_x(z) = \omega_x(1) + [\omega_x(z_g) - \omega_x(1)]C_x(z, z_g) \end{cases} \quad (4)$$

From the matching to the number-of-layer dependence, we can derive the $\omega_x(1)$, the $\omega_x(z)$, and the correlation between the n and the effective z of the n -layered graphene.

Similarly, the strain-effect is given as,

$$\begin{aligned} \frac{\omega_x(z, \varepsilon) - \omega_x(1, 0)}{\omega_x(z, 0) - \omega_x(1, 0)} &= \frac{d_z}{d(z, \varepsilon)} \left(\frac{E(z, \varepsilon)}{E_z} \right)^{1/2} = \frac{\left(1 - d_z^2 \int_0^\varepsilon \kappa \varepsilon d\varepsilon / E_z \right)^{1/2}}{1 + \varepsilon} \\ &\cong \frac{\left(1 - \kappa' (\lambda \varepsilon')^2 \right)^{1/2}}{1 + \lambda \varepsilon'} \end{aligned} \quad (5)$$

with $\kappa' = \kappa d_z^2 / (2E_z) = \text{const.}$

In order to reflect the asymmetric responses of the C_{3v} bond geometry to the applied C_{2v} strain, we introduced a strain coefficient λ bounded by $0 \leq \lambda \leq 1$. The $\varepsilon = \lambda \varepsilon'$ is for the branch responding less to the applied strain. $\kappa = 2E_z \kappa' d_z^{-2}$ is the effective force constant of all the C_{3v} bonds of a given atom. Practically, one can measure the average strain of the entire specimen other than that of the individual bond with a force constant κ_0 . Because of the C_{3v} symmetry of the graphene, the applied uni-axial or bi-axial strain differentiates the actual strains of the three bonds in the graphene. The magnitudes of the strain and the strain energy of each bond should vary with the relative direction between the strain and the crystal orientation. It is therefore not surprising that the mechanical strain induces phonon band splitting.

By definition, we can derive the Grüneisen parameter from (5),

$$\gamma_E = -\frac{\partial \ln \omega'}{\partial \ln \varepsilon} = \varepsilon \left[\frac{1 + \kappa' \varepsilon}{(1 - \kappa' \varepsilon^2)(1 + \varepsilon)} \right]$$

$$\text{or, } \gamma'_E = -\frac{\partial \omega'}{\partial \varepsilon} = \frac{1 + \kappa' \varepsilon}{(1 - \kappa' \varepsilon^2)^{1/2} (1 + \varepsilon)^2}$$

$$\text{With } \omega' = \frac{\omega_x(z, \varepsilon) - \omega_x(1, 0)}{\omega_x(z, 0) - \omega_x(1, 0)}$$

(6)

From matching the strain dependent, we can derive the force constant of the C-C bond and the strain coefficient λ , without needing the Grüneisen parameter that is not a constant as a matter of fact.

2.5 Pressure and temperature dependence

Likewise, using the approximation $1 + x \cong \exp(x)$ at $x \ll 1$, we can formulate the thermal and pressure effects,[53]

$$\frac{\omega(z, y) - \omega(1, y_0)}{\omega(z, y_0) - \omega(1, y_0)} \cong \begin{cases} (1 - \Delta_T)^{1/2} \exp\left(\int_{T_0}^T \alpha dt\right) \\ (1 + \Delta_P)^{1/2} \exp\left(\int_{P_0}^P \beta dp\right) \end{cases} \quad (y = T, P)$$

(7)

The thermally- and mechanically-induced energy perturbations Δ_T and Δ_P follow the relations,

[32]

$$\Delta_T = \int_{T_0}^T \frac{\eta(t) dt}{E_z} = \int_0^T \frac{C_V(T/\theta_D)}{zE_z} dt = \int_0^T \frac{4R(T/\theta_D)^2 \int_0^{\theta_D/T} (e^x - 1)^{-1} x^2 dx}{E_{coh}} dt$$

$$\Delta_P = -\int_{V_0}^V \frac{p(v) dv}{E_z} = -\frac{V_0}{E_z} \int_1^x p(x) dx = -\int_1^x \frac{p(x) dx}{E_{den}}$$

$$\text{with } \begin{cases} p(x) = 3/2 \times B_0 (x^{-7/3} - x^{-5/3}) (1 + 3(B_0' - 4)(x^{-2/3} - 1)/4) & (BM) \\ x(P) = V/V_0 = 1 - \beta P + \beta' P^2 & (Non-linear) \end{cases}$$

(8)

The Δ_T is the integral of the specific heat reduced by the bond energy in two-dimensional Debye approximation. When the measuring temperature T is higher than θ_D , the two-dimensional specific heat C_v approaches a constant of $2R$ (R is the idea gas constant). The atomic cohesive energy $E_{coh} = zE_z$ and the θ_D are the uniquely adjustable parameters in calculating the Δ_T . The Δ_P is calculated based on the integral of the Birch-Mürnaghan (BM) equation,[54, 55] or the $x(p)$. V_0 is the initial volume of a bond. The variables in Δ_P are the binding energy density $E_{den} = E_z / V_0$ and the compressibility β and β' . The $x(P)$ is another form of the equation of states in terms of the nonlinear compressibility. Matching the BM equation to the $x(P)$ or the measured x - P curve, one can derive the nonlinear compressibility β and β' , the bulk modulus B_0 ($\beta B_0 \cong 1$) and its first-order differentiation B'_0 . Substituting the integrals (8) into (7), we can reproduce the P - and T -dependent Raman shift with derivatives of the θ_D , α , and E_{den} and the compressibility derived from the $x(P)$ relation with the known E_{coh} .

3. Experimental and calculation procedures

The well established Raman database as functions of the number-of-layer,[3, 22] compressive [5, 25] and tensile[25] strain, temperature,[56] and pressure [8] enabled the verification of the derived formulations and expectations. In numerical calculations, the known effective bond length $d_g = 0.142$ nm and $z_g = 5.335$ for the bulk graphite, $z = 3$ for the single layer graphene, and the $m = 2.56$ for carbon were taken as input parameters. We assumed the experimental database is sufficiently accurate. Errors in measurements will render the accuracy of the derivatives but not the nature and the trends of the observations.

We firstly calculated the ω - z curves and calibrate them with the known vibration frequencies for the bulk graphite and the monolayer graphene. This calibration leads to the quantification of

$\omega_x(1)$. Based on the z -dependent ω - z curve, we can determine the correlation between the effective atomic CN and the number-of-layer n for the few-layer graphene of all the possible modes. Likewise, matching to the strain-dependent Raman shifts and the strain-induced band splitting, we can determine the force constant and the effective strain for different branches of the splitting band. Matching to the T- and P-dependence, we can obtain the θ_D , E_{coh} , E_{den} and β and β' values without involving any other adjustable parameters. We have thus unified, for the first time, the Raman shifts of various modes under the considered stimuli, which have not been realized by any other approaches.

4. Results and discussion

4.1 Number-of-layer dependence

With the given Raman frequencies of the 2D peak shifting from 2720 to 2680 cm^{-1} and the D peak from 1367 to 1344 cm^{-1} when the graphite (z_g) turns to be the monolayer ($z = 3$) graphene,[3, 22, 57] and the G mode shifting from 1582 to 1587 cm^{-1} , [3, 4] we can calibrate the z -dependent relative shift of the possible modes,

$$C_x(z, z_g) = \frac{\omega_x(z) - \omega_x(1)}{\omega_x(z_g) - \omega_x(1)} = \left(\frac{C_z}{C_{z_g}} \right)^{-2.28} \begin{cases} \frac{z}{z_g} & (D, 2D) \\ 1 & (G) \end{cases} \text{ and,}$$

$$C_x(3, z_g) = \left(\frac{0.8147}{0.9220} \right)^{-2.28} \times \begin{cases} \frac{3.0}{5.335} & = 0.7458 (D, 2D) \\ 1 & = 1.3260 (G) \end{cases} .$$

The reference frequencies and the general expression for the z -dependency are derived as,

$$\omega_x(1) = \frac{\omega_x(3) - \omega_x(z_g) C_x(3, z_g)}{1 - C_x(3, z_g)} = \begin{cases} 1276.8 & (D) \\ 2562.6 & (2D) \\ 1566.7 & (G) \end{cases} (\text{cm}^{-1})$$

$$\begin{aligned}\omega_x(z) &= \omega_x(1) + [\omega_x(z_g) - \omega_x(1)]C_x(z, z_g) \\ &= \begin{cases} 1276.8 + 90.2 \times C_D(z, z_b) & (D) \\ 2562.6 + 157.4 \times C_D(z, z_b) & (2D) \\ 1566.7 + 16.0 \times C_G(z, z_b) & (G) \end{cases} (cm^{-1})\end{aligned}$$

(9)

Figure 1 shows the modeling reproduction of the z dependence Raman frequencies of (a) the D/2D modes [3, 5, 25] and (b) the G mode. The inset in (b) shows the original experimental ω -n data for the G mode.[3, 4] Panel (c) is the z - n transformation derived from (a) and (b). It is seen that when the n is greater than 6, the z reaches and then maintains almost the bulk graphite value of 5.335. The consistency between predictions and the measurements of the z-dependent Raman shifts and the z-n transformation function for the three modes evidences the essentiality and appropriateness of the proposed mechanisms for the lattice vibration in graphene.

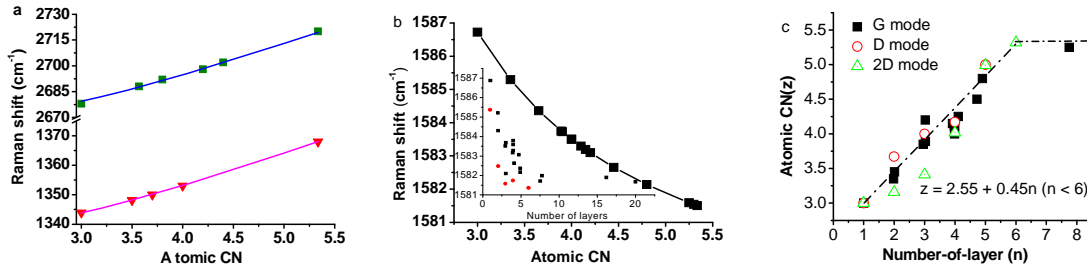


Figure 1 BOLS reproduction of the z dependence of the (a) D/2D modes [3, 22] and the (b) G mode Raman frequency with derivative of the referential vibration frequency of each. The inset in (b) shows the originally experimental ω -n data for the G mode.[3, 4] Panel (c) shows the correlation function between the atomic CN and the number-of-layer. For $n > 6$, the z approaches and maintains almost the bulk graphite value of 5.335.

4.2 Strain-induced red shifting and band splitting

Combining eq (5) and (9), we have the joint z - and ε -dependent Raman shifts:

$$\begin{aligned} \omega_x(z, \varepsilon) &= \omega_x(1,0) + [\omega_x(z_g,0) - \omega_x(1,0)] C_x(z, z_g) \times (1 - \kappa'(\lambda\varepsilon)^2)^{1/2} \times (1 + \lambda\varepsilon)^{-1} \\ &= \begin{matrix} 1276.8 \\ 2562.6 \\ 1566.7 \end{matrix} \left. \vphantom{\omega_x(z, \varepsilon)} \right\} + C_x(z, z_g) \frac{(1 - \kappa'(\lambda\varepsilon)^2)^{1/2}}{1 + \lambda\varepsilon} \times \begin{matrix} 90.2 & (D) \\ 157.4 & (2D) \\ 16.0 & (G) \end{matrix} (cm^{-1}) \end{aligned} \quad (10)$$

Figure 2 shows the (a) uni-axial compressive [5, 25] and tensile[25] strain induced D/2D mode red shifting without band splitting and the (b) tensile strain induced 2D mode red shifting and band splitting.[24] For all the D/2D and G modes, the reduced force constant

$\kappa' = \kappa d_z^2 / (2E_z) = 0.30$, has been derived, corresponding to $\kappa = 6.283$ N/m for graphene ($z = 3$).

The inset in (a) illustrates the asymmetric response of the three bonds of C_{3v} group symmetry, denoted 1, 2, and 3, to the uni-axial tensile strain. There are two extreme situations: at $\theta = 0^\circ$, or the strain is along bond 2, $\varepsilon_1 = \varepsilon_3 = \lambda\varepsilon_2 < \varepsilon_2$; at $\theta = 30^\circ$, or the strain is perpendicular to bond 3, $\varepsilon_1 = \varepsilon_2 > \varepsilon_3 \sim 0$. The ε_2 seems to be the maximum at $\theta = 0^\circ$. The bond configuration symmetry allows us to focus on the angle ranging from 0° to 30° between a specific bond and the strain. There should be a branch remaining the original frequency as $\varepsilon_3 \sim 0$ at $\theta = 30^\circ$ in panel (a); panel (b) should correspond to $\theta = 0^\circ$ with band splitting.

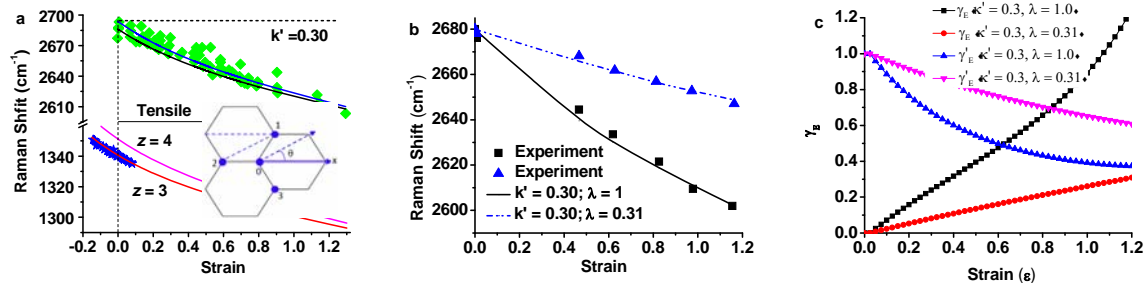


Figure 2 BOLS reproduction of (a) the uni-axial compressive[5, 25] and tensile[25] strain induced Raman shift of the D/2D bands and (b) the tensile strain induced 2D band red shifting and band splitting.[24] The inset in (a) illustrates the anisotropic response of the C_{3v} bonds to the uni-axial strain. There are two extreme situations: at $\theta = 0^\circ$, $\varepsilon_1 = \varepsilon_3 = \lambda\varepsilon_2 < \varepsilon_2$; at $\theta = 30^\circ$, $\varepsilon_1 = \varepsilon_2 > \varepsilon_3 \sim 0$. The reduced force constant $\kappa' = 0.3$ and the effective strain of the slow-shifted branch in (b) $\varepsilon' = \lambda\varepsilon$. There should be a constant branch in (a) if $\theta = 30^\circ$. The 2D mode in panel (a) appears to correspond to $\theta = 30^\circ$ needing a constant branch because $\varepsilon_3 \sim 0$ and (b) to 0° situation. Panel (c) and eq (6) show the Grüneisen parameters for the diverged branches of the 2D mode in (b).

In addition to the Grüneisen parameters derived in eq (6), we employed the strain coefficient λ for the strain-induced red shifting and band splitting. The introduction of the λ and the κ is more convenient and physically meaningful than using the Grüneisen parameter alone. In panel (b), the $\lambda = 0.31$ for the upper and $\lambda = 1.0$ for the lower branches. This result means that the bonds labeled 1 and 3 in the inset are elongated by 31% of that of the bond 2 if the strain is along bond 2. As the λ changes with the relative direction between the strain and the crystal orientation, any possible extent of splitting and frequency variation with strain can be reproduced, which could further explain how the “two-phonon double-resonance” proceeds under the given circumstances.

From the C_{3v} bond configuration shown as inset in Figure 2a, and the derived effective force constant $\kappa = 6.283$ N/m, we can estimate the force constant of the C-C bond in the single layer graphene. We may define the C-C bond force constant k_0 , the bonds labeled 1 and 3 are approximated as in parallel and the resultant $\kappa_{13} = 2\kappa_0$. This resultant bond connects with bond 2

in series and therefore the resultant force constant of the three bonds is $\kappa_{123} = \kappa = 2\kappa_0/3$. Hence, the C-C bond force constant $\kappa_0 = 3\kappa_0/2 \sim 9.424$ N/m.

4.3 Pressure and temperature dependence

The matching to the measured T-dependent Raman shift of the 2D mode in Figure 3a turns out that $\theta_D = 540$ K, with the given atomic cohesive energy of 3.11 eV/atom. The θ_D is about 1/3 fold of the melting point 1605 K for the SWCNT.[30] At $T \sim \theta_D/3$, the Raman shift turns gradually from the nonlinear to the linear form when the temperature is increased. The slow decrease of the Raman shift at very low temperatures arises from the small $\int_0^T \eta dt$ values as the specific heat $\eta(t)$ is proportional to T^2 for the two-dimensional system at very low temperatures. These results imply that the θ_D determines the width of the shoulder and the $1/E_{coh}$ and the thermal expansion coefficient determine the slope of the curve at high temperatures. The match to the measured P-dependent Raman shift in Figure 3b gives rise to the compressibility of $\beta = 1.145 \times 10^{-3}$ (GPa⁻¹) and $\beta' = 7.63 \times 10^{-5}$ (GPa⁻²) and the energy density of 320 eV/nm³.

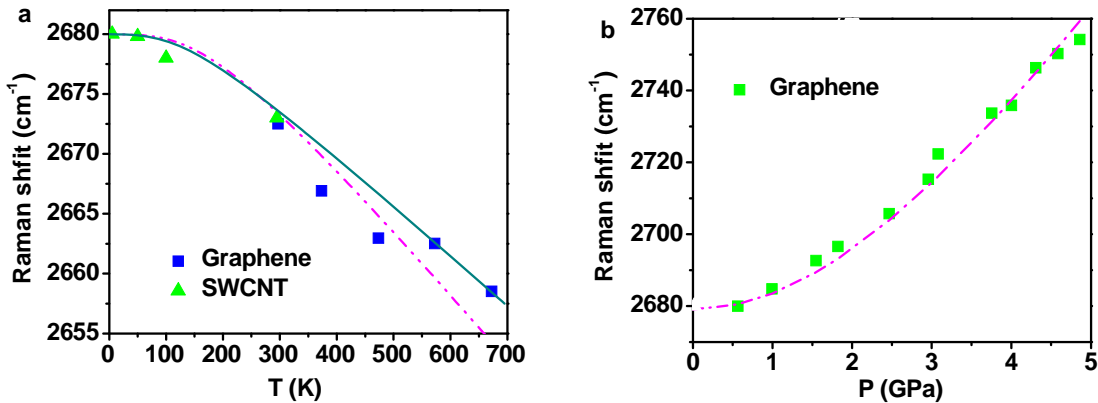


Figure 3 BOLS reproduction of the measured (a) temperature [56] and (b) pressure [8] dependent Raman shift of the 2D mode of graphene and CNT gives rise to the Debye temperature of 504 K

with the given atomic cohesive energy of 3.11 eV/atom, and the compressibility and energy density as given in Table 1.

Table 1 Instrumental information derived from the reproduction of the ϵ -, T-, and P-dependent Raman shift of monolayer graphene.

Stimuli	Quantities	Values	Refs
Number-of-layer	$\omega_x(1)$	$\begin{cases} 1276.8 & (D) \\ 2562.6 & (2D)(\text{cm}^{-1}) \\ 1566.7 & (G) \end{cases}$	-
	$\omega(z_g) - \omega(1)$	$\begin{cases} 90.2 & (D) \\ 157.4 & (2D)(\text{cm}^{-1}) \\ 16.0 & (G) \end{cases}$	-
Strain	κ (Nm ⁻¹)	6.283	-
Temperature	E_{coh} (eV/atom)	3.11	-
	θ_D (K)	540	$T_m = 1605$ [30]
	α (10 ⁻⁶ K ⁻¹)	9.0	-
Pressure	E_{den} (eV/nm ³)	320	-
	β/β' (10 ⁻³ GPa ⁻¹ /GPa ⁻²)	1.145/0.0763	-
	B_0/B'_0 (GPa/-)	690/5	704/1[58]

4.4 Edge discriminative Raman reflectivity

Recent progress [29] confirmed that the Dirac-Fermi polarons preferentially generate at the zigzag-edge of graphene[59] and at graphite surface atomic vacancies[60] because of the longer and uniform $\sqrt{3}d$ distance between the dangling bond electrons along the edge. As illustrated in Figure 4, the dangling bond electrons at the edges of the armchair- and the reconstructed zigzag graphene (5 and 7 atomic rings) tend to form quasi-triple-bond between the

edge atoms of shorter d distance. The isolation and polarization of the unpaired dangling bond electrons at the zigzag edge by the locally and deeply entrapped core and bonding electrons may scatter the incident radiation substantially and hence lowers the Raman reflectivity of the D band at the zigzag edge compared with that at the arm-chaired edge.[18, 19]

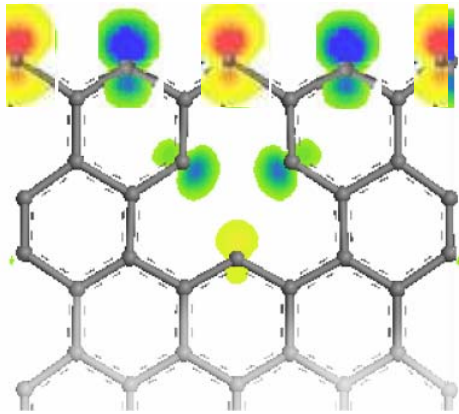


Figure 4 Density function theory calculated preferential generation of the DFPs with alternative directions (different colors) of spins at the zigzag edge and atomic vacancy of graphene. The DFPs are recognized as the isolation and polarization of the dangling bond electrons by the densely entrapped bonding electrons of the undercoordinated edge atoms that are separated by $\sqrt{3}d$ along the zigzag edge uniformly. The shorter d separation of the dangling bond electrons form quasi-triple-bond without being polarized along the arm-chair edge.[29]

5. Conclusion

We have formulated, for the first time, the number-of-layer, uni-axial-strain, pressure, and temperature dependent Raman shifts of graphene, as a union, as a function depending on the BOLS correlation in terms of the response of the length and energy of the representative bond to the applied stimuli. Numerical reproduction of the measurements clarified that: (i) the number-

of-layer induced D and 2D redshift and the G mode blueshift are ruled by different mechanisms resulting from the undercoordination induced bond strain and bond strength gain; The D/2D vibration involves all the z neighbors on a C atom while the G mode involve only a dimer; (ii) the strain-induced phonon softening and band splitting arise from the anisotropic bond elongation and bond weakening; (iii) the thermally-softening originates from bond expansion and bond weakening due to vibration; and (iv) the mechanically-stiffening results from bond compression and bond strengthening due to mechanical work hardening. Reproduction of the measurements has led to quantitative information, as summarized in Table 1, of the referential frequencies for each mode from which the Raman shifts proceed, the bond length, bond energy, atomic cohesive energy, binding energy density, force constant, Debye temperature, compressibility, elastic modulus of graphene, and the effective coordination numbers for the few-layer graphene, which is of instrumental importance to the understanding of the unusual behavior of graphene. Findings and understandings demonstrate the essentiality of the proposed approach that has empowered the Raman spectroscopy immensely in gaining quantitative information about the dynamics of the representative bond of a specimen.

Acknowledgements

Financial supports from NSF (Nos. 50832001 and 11172254) of China and MOE (RG15/09), Singapore, are gratefully acknowledged.

References

- [1] Hao Y, Wang Y, Wang L, Ni Z, Wang Z, Wang R, Koo CK, Shen Z, and Thong JTL, *Probing Layer Number and Stacking Order of Few-Layer Graphene by Raman Spectroscopy*. Small, 2010; **6**: 195-200.
- [2] Wang H, Wang Y, Cao X, Feng M, and Lan G, *Vibrational properties of graphene and graphene layers*. Journal of Raman Spectroscopy, 2009; **40**: 1791-1796.
- [3] Graf D, Molitor F, Ensslin K, Stampfer C, Jungen A, Hierold C, and Wirtz L, *Spatially Resolved Raman Spectroscopy of Single- and Few-Layer Graphene*. Nano Letters, 2007; **7**: 238-242.
- [4] Gupta A, Chen G, Joshi P, Tadigadapa S, and Eklund PC, *Raman Scattering from High-Frequency Phonons in Supported n-Graphene Layer Films*. Nano Letters, 2006; **6**: 2667-2673.
- [5] Mohiuddin TMG, Lombardo A, Nair RR, Bonetti A, Savini G, Jalil R, Bonini N, Basko DM, Galiotis C, Marzari N, Novoselov KS, Geim AK, and Ferrari AC, *Uniaxial strain in graphene by Raman spectroscopy: G peak splitting, Gruneisen parameters, and sample orientation*. Phys Rev B, 2009; **79**: 205433.
- [6] Yu T, Ni Z, Du C, You Y, Wang Y, and Shen Z, *Raman Mapping Investigation of Graphene on Transparent Flexible Substrate: The Strain Effect*. The Journal of Physical Chemistry C, 2008; **112**: 12602-12605.
- [7] Huang M, Yan H, Heinz TF, and Hone J, *Probing Strain-Induced Electronic Structure Change in Graphene by Raman Spectroscopy*. Nano Letters, 2010; **10**: 4074-4079.
- [8] Proctor JE, Gregoryanz E, Novoselov KS, Lotya M, Coleman JN, and Halsall MP, *High-pressure Raman spectroscopy of graphene*. Physical Review B, 2009; **80**: 073408-073412.
- [9] Calizo I, Ghosh S, Bao W, Miao F, Ning Lau C, and Balandin AA, *Raman nanometrology of graphene: Temperature and substrate effects*. Solid State Communications, 2009; **149**: 1132-1135.
- [10] Dattatray JL, Maitra U, Panchakarla LS, Waghmare UV, and Rao CNR, *Temperature effects on the Raman spectra of graphenes: dependence on the number of layers and doping*. J. Phys.: Condens. Matter, 2011; **23**: 055303.
- [11] Martins Ferreira EH, Moutinho MVO, Stavale F, Lucchese MM, Capaz RB, Achete CA, and Jorio A, *Evolution of the Raman spectra from single-, few-, and many-layer graphene with increasing disorder*. Physical Review B, 2010; **82**: 125429-125438.
- [12] Berciaud S, Ryu S, Brus LE, and Heinz TF, *Probing the Intrinsic Properties of Exfoliated Graphene: Raman Spectroscopy of Free-Standing Monolayers*. Nano Letters, 2008; **9**: 346-352.

- [13] Calizo I, Bao W, Miao F, Lau CN, and Balandin AA, *The effect of substrates on the Raman spectrum of graphene*. Applied Physics Letters, 2007; **91**: 201904.
- [14] Luo Z, Yu T, Kim KJ, Ni Z, You Y, Lim S, Shen Z, Wang S, and Lin J, *Thickness-Dependent Reversible Hydrogenation of Graphene Layers*. ACS Nano, 2009; **3**: 1781-1788.
- [15] Xie LM, Jiao LY, and Dai HJ, *Selective Etching of Graphene Edges by Hydrogen Plasma*. J. Am. Chem. Soc., 2010; **132**: 14751-14753.
- [16] Shin HJ, Choi WM, Choi D, Han GH, Yoon SM, Park HK, Kim SW, Jin YW, Lee SY, Kim JM, Choi JY, and Lee YH, *Control of Electronic Structure of Graphene by Various Dopants and Their Effects on a Nanogenerator*. J. Am. Chem. Soc., 2010; **132**: 15603-15609.
- [17] Cancado LG, Pimenta MA, Neves BRA, Dantas MSS, and Jorio A, *Influence of the Atomic Structure on the Raman Spectra of Graphite Edges*. Physical Review Letters, 2004; **93**: 247401-247405.
- [18] Krauss B, Nemes Incze P, Skakalova V, Biro LP, Klitzing KV, and Smet JH, *Raman Scattering at Pure Graphene Zigzag Edges*. Nano Letters, 2010; **10**: 4544-4548.
- [19] You Y, Ni Z, Yu T, and Shen Z, *Edge chirality determination of graphene by Raman spectroscopy*. Applied Physics Letters, 2008; **93**: 163112-163115.
- [20] Pimenta MA, Dresselhaus G, Dresselhaus MS, Cancado LG, Jorio A, and Saito R, *Studying disorder in graphite-based systems by Raman spectroscopy*. Physical Chemistry Chemical Physics, 2007; **9**: 1276-1290.
- [21] Dresselhaus MS, Jorio A, and Saito R, *Characterizing Graphene, Graphite, and Carbon Nanotubes by Raman Spectroscopy*. Annual Review of Condensed Matter Physics, 2010; **1**: 89-108.
- [22] Gupta AK, Russin TJ, Gutierrez HR, and Eklund PC, *Probing Graphene Edges via Raman Scattering*. ACS Nano, 2008; **3**: 45-52.
- [23] Calizo I, Balandin AA, Bao W, Miao F, and Lau CN, *Temperature Dependence of the Raman Spectra of Graphene and Graphene Multilayers*. Nano Letters, 2007; **7**: 2645-2649.
- [24] Yoon D, Son Y-W, and Cheong H, *Strain-Dependent Splitting of the Double-Resonance Raman Scattering Band in Graphene*. Phys. Rev. Lett., 2011; **106**: 155502.
- [25] Ding F, Ji H, Chen Y, Herklotz A, Dorr K, Mei Y, Rastelli A, and Schmidt OG, *Stretchable Graphene: A Close Look at Fundamental Parameters through Biaxial Straining*. Nano Letters, 2010; **10**: 3453-3458.
- [26] Liu J and Vohra YK, *Raman Modes of 6H Polytype of Silicon Carbide to Ultrahigh Pressures: A Comparison with Silicon and Diamond*. Physical Review Letters, 1994; **72**: 4105-4108.

- [27] Cuscó R, Alarcón Lladó E, Ibáñez J, Artús L, Jiménez J, Wang B, and Callahan MJ, *Temperature dependence of Raman scattering in ZnO*. Physical Review B, 2007; **75**: 165202-165213.
- [28] Sun CQ, *Size dependence of nanostructures: Impact of bond order deficiency*. Progress in Solid State Chemistry, 2007; **35**: 1-159.
- [29] Zhang X, Zheng WT, Kuo J-L, and Sun CQ, *Discriminative generation and hydrogen modulation of the Dirac-Fermi polarons at graphene edges and atomic vacancies*. Carbon, 2011; **49**: 3615-3621.
- [30] Sun CQ, Bai HL, Tay BK, Li S, and Jiang EY, *Dimension, strength, and chemical and thermal stability of a single C-C bond in carbon nanotubes*. J. Phys. Chem. B, 2003; **107**: 7544-7546.
- [31] Sun CQ, Sun Y, Nie YG, Wang Y, Pan JS, Ouyang G, Pan LK, and Sun Z, *Coordination-Resolved C-C Bond Length and the C 1s Binding Energy of Carbon Allotropes and the Effective Atomic Coordination of the Few-Layer Graphene*. J Chem Phys C, 2009; **113**: 16464-16467.
- [32] Sun CQ, *Thermo-mechanical behavior of low-dimensional systems: The local bond average approach*. Prog. Mater Sci., 2009; **54**: 179-307.
- [33] Goldschmidt VM, *Crystal structure and chemical correlation*. Berichte Der Deutschen Chemischen Gesellschaft, 1927; **60**: 1263-1296.
- [34] Pauling L, *Atomic radii and interatomic distances in metals*. J. Am. Chem. Soc., 1947; **69**: 542-553.
- [35] Feibelman PJ, *Relaxation of hcp(0001) surfaces: A chemical view*. Phys Rev B, 1996; **53**: 13740-13746.
- [36] Miller JT, Kropf AJ, Zha Y, Regalbuto JR, Delannoy L, Louis C, Bus E, and van Bokhoven JA, *The effect of gold particle size on Au-Au bond length and reactivity toward oxygen in supported catalysts*. J. Catal., 2006; **240**: 222-234.
- [37] Huang WJ, Sun R, Tao J, Menard LD, Nuzzo RG, and Zuo JM, *Coordination-dependent surface atomic contraction in nanocrystals revealed by coherent diffraction*. Nat. Mater., 2008; **7**: 308-313.
- [38] Petkov V, Peng Y, Williams G, Huang BH, Tomalia D, and Ren Y, *Structure of gold nanoparticles suspended in water studied by x-ray diffraction and computer simulations*. Phys Rev B, 2005; **72**: 195402.
- [39] Yang DQ and Sacher E, *Initial- and final-state effects on metal cluster/substrate interactions, as determined by XPS: copper clusters on Dow Cyclotene and highly oriented pyrolytic graphite*. Appl. Surf. Sci., 2002; **195**: 187-195.

- [40] Aruna I, Mehta BR, Malhotra LK, and Shivaprasad SM, *Size dependence of core and valence binding energies in Pd nanoparticles: Interplay of quantum confinement and coordination reduction*. J. Appl. Phys., 2008; **104**: 064308-064305.
- [41] Kittel C, *Introduction to Solid State Physics*. Wiley: New York, 1996: pp 57.
- [42] Wong EW, Sheehan PE, and Lieber CM, *Nanobeam Mechanics: Elasticity, Strength, and Toughness of Nanorods and Nanotubes*. Science, 1997; **277**: 1971-1975.
- [43] Falvo MR, Clary GJ, Taylor RM, Chi V, Brooks Jr FP, Washburn S, and Superfine R, *Bending and buckling of carbon nanotubes under large strain*. Nature, 1997; **389**: 582-584.
- [44] Bai A, Seiji F, Kiyoshi Y, and Masamichi Y, *Surface Superstructure of Carbon Nanotubes on Highly Oriented Pyrolytic Graphite Annealed at Elevated Temperatures*. Jpn. J. Appl. Phys. , 1998; **37**: 3809-3811.
- [45] Balasubramanian T, Andersen JN, and Wallden L, *Surface-bulk core-level splitting in graphite*. Physical Review B, 2001; **64**: 205420-205423.
- [46] Kim K, Lee H, Choi JH, Youn YS, Choi J, Lee H, Kang TH, Jung MC, Shin HJ, Lee HJ, Kim S, and Kim B, *Scanning Photoemission Microscopy of Graphene Sheets on SiO₂*. Advanced Materials, 2008; **20**: 3589-3591.
- [47] Zheng WT and Sun CQ, *Underneath the fascinations of carbon nanotubes and graphene nanoribbons*. Energy & Environmental Science, 2011; **4**: 627-655.
- [48] Kreisel KA, Yap GPA, Dmitrenko O, Landis CR, and Theopold KH, *The shortest metal-metal bond yet: Molecular and electronic structure of a dinuclear chromium diazadiene complex*. J. Am. Chem. Soc., 2007; **129**: 14162-+.
- [49] Cotton FA, Hillard EA, Murillo CA, and Zhou HC, *After 155 years, a crystalline chromium carboxylate with a supershort Cr-Cr bond*. J. Am. Chem. Soc., 2000; **122**: 416-417.
- [50] Girit CÖ, Meyer JC, Ermi R, Rossell MD, Kisielowski C, Yang L, Park CH, Crommie MF, Cohen ML, Louie SG, and Zettl A, *Graphene at the Edge: Stability and Dynamics*. Science, 2009; **323**: 1705-1708.
- [51] Han WG and Zhang CT, *A THEORY OF NONLINEAR STRETCH VIBRATIONS OF HYDROGEN-BONDS*. J. Phys.: Condens. Matter, 1991; **3**: 27-35.
- [52] Liu X, Pan L, Sun Zhuo, and Sun C, Q., *Strain engineering of the elasticity and the Raman shift of nanostructured TiO₂*. J. Appl. Phys., 2011; **accepted on 16/07/2011**.
- [53] Gu MX, Pan LK, Au Yeung TC, Tay BK, and Sun CQ, *Atomistic Origin of the Thermally Driven Softening of Raman Optical Phonons in Group III Nitrides*. The Journal of Physical Chemistry C, 2007; **111**: 13606-13610.
- [54] Birch F, *Finite Elastic Strain of Cubic Crystals*. Physical Review, 1947; **71**: 809-824.

- [55] Murnaghan FD, *The Compressibility of Media under Extreme Pressures*. Proceedings of the National Academy of Sciences of the United States of America, 1944; **30**: 244-247.
- [56] Zhang L, Jia Z, Huang L, O'Brien S, and Yu Z, *Low-Temperature Raman Spectroscopy of Individual Single-Wall Carbon Nanotubes and Single-Layer Graphene*. The Journal of Physical Chemistry C, 2008; **112**: 13893-13900.
- [57] Thomsen C and Reich S, *Double Resonant Raman Scattering in Graphite*. Physical Review Letters, 2000; **85**: 5214-5217.
- [58] Reich S, Thomsen C, and Ordejon P, *Elastic properties of carbon nanotubes under hydrostatic pressure*. Physical Review B, 2002; **65**: 153407-153411.
- [59] Enoki T, Kobayashi Y, and Fukui KI, *Electronic structures of graphene edges and nanographene*. Int. Rev. Phys. Chem., 2007; **26**: 609-645.
- [60] Ugeda MM, Brihuega I, Guinea F, and Gómez-Rodríguez JM, *Missing Atom as a Source of Carbon Magnetism*. Phys. Rev. Lett., 2010; **104**: 096804.